

Optical and Electrical Properties of Sol-Gel Synthesized Calcium Copper Titanate Nanopowders.

P. Thiruramanathan¹, A. Marikani^{1*}, D. Madhavan²

¹Department of Physics, Mepco Schlenk Engineering College,
Sivakasi – 626 005, Tamil Nadu, India.

²Department of Chemistry, Mepco Schlenk Engineering College,
Sivakasi – 626 005, Tamil Nadu, India.

Abstract: In this paper, we have investigated the optical and electrical properties of calcium copper titanate ($\text{CaCu}_3\text{Ti}_4\text{O}_{12}$) (CCTO) nanopowder synthesized by sol-gel combustion process. X-ray diffraction pattern has confirmed the presence of well crystalline $\text{CaCu}_3\text{Ti}_4\text{O}_{12}$ (CCTO) nanopowder with perovskite structure. The intensity of preferential orientation (2 2 0) increases with increasing the calcinations temperature and attained monophasic at 800°C for 3 hours. The observed characteristic bands in the fourier transform infra-red spectrum confirmed perovskite CCTO. The nature of surface morphology was studied using scanning electron microscopy and atomic force microscopy. Optical parameters like refractive index, extinction coefficient, dielectric constant, direct and indirect allowed band gap values were examined from diffused reflectance spectroscopy explained in graphical representation. Nyquist plots show the dominance of grain contribution, which allows the determination of electrical properties.

Key words: Calcium copper titanate, Sol-gel synthesis, Optical properties, Electrical properties.

Introduction:

The $\text{CaCu}_3\text{Ti}_4\text{O}_{12}$ (CCTO) was first reported by Subramanian et al.,¹. It belongs to a family of oxides of the type $\text{ACu}_3\text{Ti}_4\text{O}_{12}$ ($A=\text{Ca, Cd, Sr, Na, Th}$)² and has been known since 1967. This family was expanded and accurate structures were determined in 1979³. Its structure (space group $Im\bar{3}$) can be derived from an ideal cubic perovskite structure by superimposing a body centered ordering of Ca and Cu ions and a pronounced tilt of the titanium centered octahedral⁴. The dielectric constant of CCTO single crystal is close to 10^5 ⁵, polycrystals in the range of 10^3 - 10^6 and ceramics are more than 10^4 ⁷ over a wide range of temperature from 100-600K. In this Colossal dielectric behavior has been investigated in detail and it has been attributed to the Maxwell Wagner relaxation mechanism⁸. The high dielectric constants and low loss tangential loss materials are widely used in technological applications such as capacitors, resonators and filters. Dielectric materials can be used to store electrical energy in the form of charge separation when the electron distributions around constituent atoms or molecules are polarized by an external electric field⁹. High dielectric constants allow miniaturization of components, thus offering the opportunity to decrease the size of electronic devices¹⁰. The solid state reaction has disadvantages of chemical inhomogeneity¹¹, relatively high calcination temperature in the range of 900-1100°C¹² and this process need a very long milling time, up to 100 hours to obtain a single-phase of CCTO¹³. Among these various methods, the sol-gel method yields ultrafine powders with homogeneity in the molecular scale, inducing a fine microstructure of the sintered ceramic¹¹. This work arise to study the properties of sol-gel synthesized CCTO nanopowder calcined at different temperature and to investigate the optimum temperature for attaining monophasic. The as-prepared powders were characterized by means of XRD, FT-IR, SEM, AFM, DRS and AC impedance spectroscopy.

Experimental procedure:

All the starting precursor materials and solvents are in purity of 99% (GR Merck) except $C_{12}H_{28}O_4Ti$ with a purity of 98% (pure synthesise). The experimental procedure for preparation of $CaCu_3Ti_4O_{12}$ by the sol-gel method is clearly explained by flow chart shown in figure 1. The final product of brownish colored ash was calcined at different temperature causes for improvement of crystallization. The final product was characterized by using various analytical techniques.

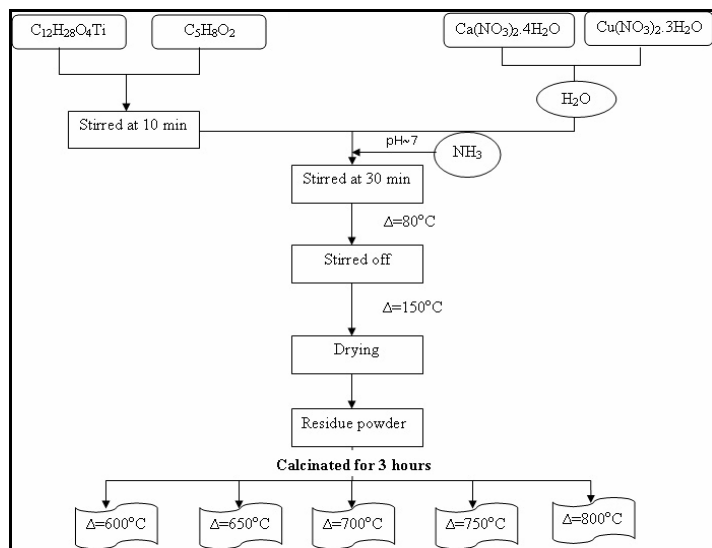


Figure 1. Flow chart for preparation of CCTO nanopowder

The structural properties of CCTO were studied using an XPERT-PRO X-ray Diffractometer with $CuK\alpha$ radiation ($\lambda = 0.15406$ nm). The functional group of CCTO was analyzed from FTIR spectrophotometer (Bruker make, Alpha-E model, Germany) in the wavenumber range from 400 to 2400 cm^{-1} . The surface morphology studies were carried out using scanning electron microscope (PHILIPS make, model-XL30) and AFM (Scanning Probe microscope, PHILIPS make, model: XL30) in non-contact mode. The calcined powders were then pressed into cylindrical pellets of 10 mm diameter and 1.4 mm thickness by applying uniform pressure about 70 MPa using a hydraulic press. It can be sintered at 950 °C for 3 hours and produced the CCTO ceramic. The palletized ceramic was placed between two copper electrodes and AC impedance analysis was done using SR830DSP Lock-in amplifier, in the frequency range 1 Hz to 100 kHz at 310 K.

Results and discussion:

The XRD pattern of as-synthesized CCTO nanopowder has shown (Fig. 2) distinct diffraction peaks which are depicted. According to S. Jesurani *et al.*,¹¹, the formation of CCTO starts when the precursor is calcined at 650 °C. It was decided to start with a calcinations temperature of 600 °C, which shows the presence of secondary phases such as $CaTiO_3$ and CuO content are also present.

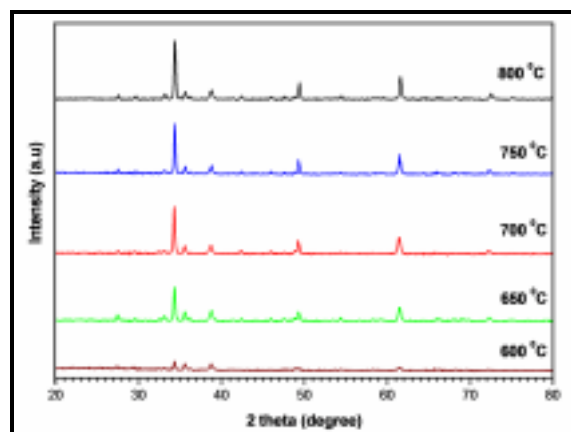


Figure 2. XRD pattern of calcium copper titanate nanopowder calcined at different temperature.

Further increasing the calcination temperature from 650 to 800 °C, the intensity of peak corresponding CaTiO_3 and CuO decreases and vanishes completely at 800 °C. The diffraction peaks along (2 2 0), (0 0 2), (0 1 3), (4 0 0) and (4 2 2) miller planes corresponded to values about 34.3, 35.6, 38.7, 49.3 and 61.59. All the observed diffraction peaks were well assigned to the cubic structure with body centered lattice of $\text{CaCu}_3\text{Ti}_4\text{O}_{12}$ [JCPDS # 752188]. At calcination temperature of 800 °C. There are no other phases present in this sample, suggests that monophasic with the high purity nature of CCTO. The intensity of the preferred orientation (2 2 0) increases with increase in calcination temperature due to their enhanced crystallinity.

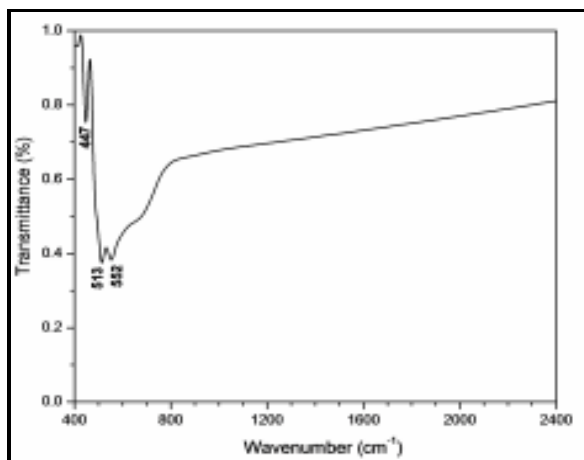


Figure 3. FTIR spectrum of CCTO powder

According to the literature survey, the formation temperature of CCTO in solid-state reaction is 1000 to 1100 °C¹⁴ and yields CCTO with the addition of some other phase such as CuO , CaTiO_3 , TiO_2 ^{1,14}. But in this case that type of problem is removed due to the superiority of this method. The crystallite size, strain¹⁵ and dislocation density of the CCTO nanopowder calcined at 800 °C were calculated to be 39.2 nm, 0.026 and 6.4×10^{14} lines/m respectively. The obtained lattice parameters $a=b=c=7.37\text{Å}$ and volume of the unit cell $399.71 (\text{Å})^3$ were similar to literature results.

The phase formation of calcium copper titanate was further confirmed from FT-IR spectrum shown in figure 3. The absorption peak corresponds to 552 cm^{-1} is related to Ca-O. The Vibrational mode of the O-Ti was appeared at 447 cm^{-1} . The absorption peak at 513 cm^{-1} is assigned to bending of Cu-O¹⁶. All the characteristic absorption bands lie in the wavenumber region of $380\text{--}700\text{ cm}^{-1}$ which once again confirms the presence of CCTO causes to mixed vibrations of CuO_4 and TiO_6 groups¹⁶.

Figure 4 (a), displays the SEM image of CCTO calcined at 800 °C. It can be revealed that the particles are present well agglomerated and not easy to define the size of distinct particles. Therefore, in this case average crystalline size (particle size) was calculated from Debye Scherer relation and about the values of 39.2 nm.

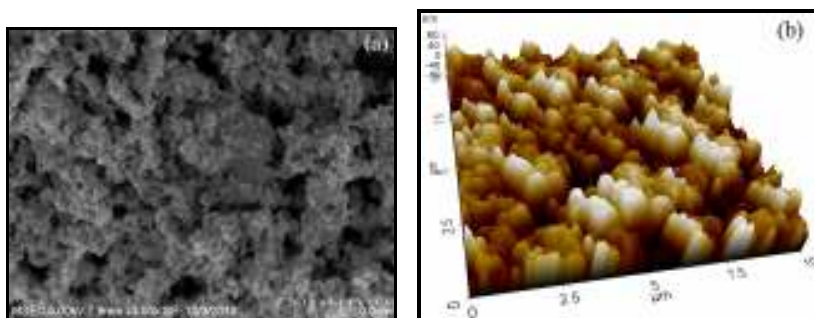


Figure 4. (a) SEM and (b) AFM image of CCTO nanopowders.

The CCTO powder was dissolved in acetone and coated on an amorphous glass substrate and record 3-D surface morphology. The AFM image (Fig.4 (b)) clearly shows that the formation of many agglomeration with different thickness depending on the chemical composition of the phases. The most used amplitude

parameters like the average roughness (R_a) and the root mean square roughness (R_q) values about 41 nm and 48 nm respectively. The functional parameters such as skewness (R_{Sk}) and kurtosis (R_{Ku}) moments are used to measure the asymmetry and the flatness, respectively. In this case, Skewness values about nearly zero (0.2), which indicates that the profile is symmetry about mean line. The Kurtosis value is smaller than three (2.1) it means that the surface is flat so called platycurtic¹⁷.

The variation of absorption coefficient with photon energy was used to find out the nature of electronic transition. The electron momentum is conserved in direct band gap and momentum is not conserved in indirect band transition¹⁸. The direct and indirect allowed transition band gap energy was evaluated from Kubelka-Munk relation¹⁹.

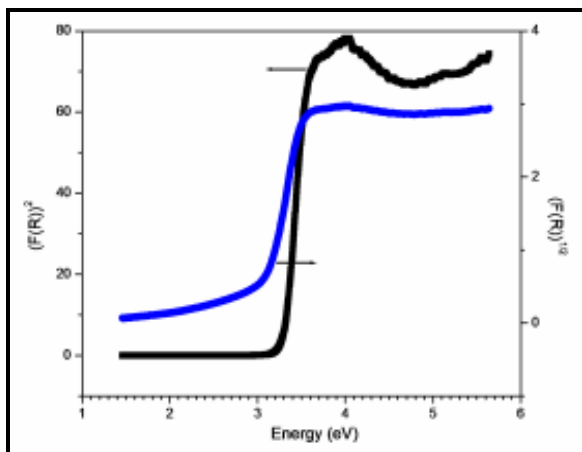


Figure 5.DRS study for band gap transitions.

The allowed direct and indirect bandgap of CCTO nanopowders was observed from plot shown in figure 5. From this figure, the direct and indirect band gap value is 3.02 and 3.25 eV respectively. Observed direct band gap value is slightly differed with a reported value of CCTO thin film as 2.88 eV²⁰. The small difference in, can be related to many factors, such as employed method, shape (powder, crystal or thin film) and synthesis conditions. Optical parameters like refractive index, extinction coefficient and dielectric constant were evaluated from reflectance spectrum²¹. The wavelength dependent refractive index and extinction coefficient of nanopowder was shown in figure 7.

The extinction coefficient is a measure of the fraction of light lost due to scattering and absorption per unit distance of the penetration medium. It is known that the refractive index is. The complex dielectric constant is a fundamental intrinsic property of the material. The real part of the dielectric constant shows how much it will slow down the speed of light in the material, whereas the imaginary part shows how a dielectric material absorbs energy from an electric field due to dipole motion²².

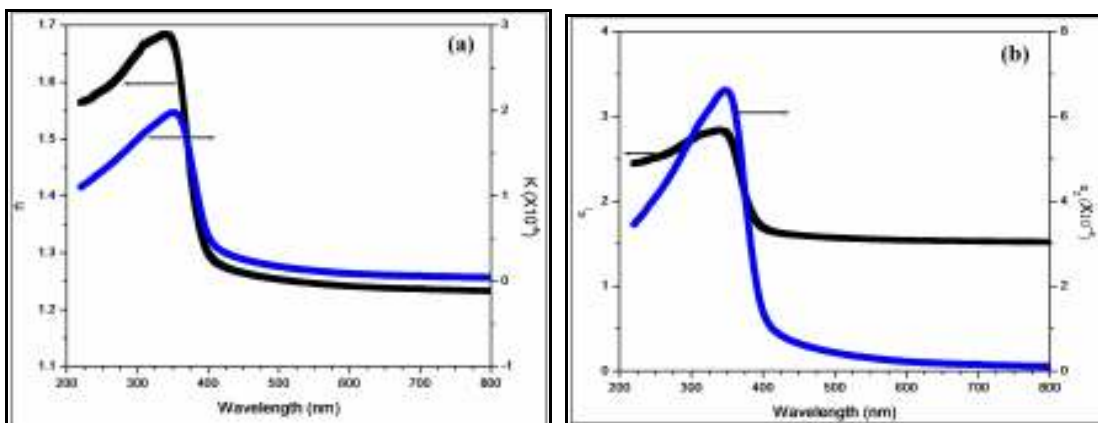


Figure 6.Variation of (a)Refractive index and extinction coefficient (b) real and imaginary part of permittivity of CCTO with wavelength

The plot of the extinction coefficient versus wavelength of incident photon energy shows that the absorptions are low in the visible region, especially for a yellow color region, which indicates that the as-synthesized powder was in the physical appearance of dark yellow in color. Figure (6 (a)) shows that the extinction coefficient decreasing with an increase in wavelength and there proves that the fraction of light lost and causes for decrease in absorbance²³.

Figure 6 (b) exhibit that optical dielectric constant of CCTO is approximately 1.5-1.6 and dielectric loss is nearly $0.2-0.3 \times 10^{-8}$ in the visible region. From IR to visible region, sudden changes in complex dielectric constant, it means that the nature of CCTO was depending on electromagnetic radiation. Hence it can be used as antenna devices. The complex impedance spectroscopy (CIS) was used to classify the real and imaginary components of the complex impedance and related parameters, and it can provide the information about the relationship between the structure-property of the ceramics. In this frequency dependent electrical parameters are related by four formalisms.

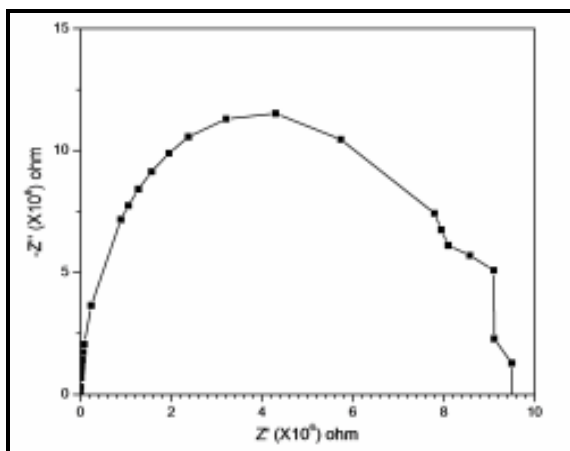


Figure 7. Nyquist plot of CCTO ceramic sintered at 950 °C for 3 hour.

The Nyquist plot (Z' vs Z'') of an as-prepared CCTO ceramic over a frequency region of 1 Hz-100 KHz at temperature 310 K is shown in figure 7. The polycrystalline materials usually have two semi-circle arcs in Nyquist plot, but in this case a single arc is observed. Subrat K. Barik et al.,²⁴ reported that the second semicircle arc appeared only if the temperature is above 250 °C.

The appearance of single semicircle provided the information about CCTO has a single polarization mechanism corresponds to the bulk or grain effects. The composition of CCTO ceramic can be described by one bulk resistance and one bulk capacitance both are connected in parallel due to the semi-circle arc is originating at the origin point. The intercept of single arc on the real axis in the higher frequency region tells about a bulk resistance (R_b). The bulk dielectric constant and DC electrical conductivity was are thickness dependent electrical properties of the material. From these relations, electrical parameters were evaluated from impedance spectrum are as follows: bulk resistance (R_b) $\sim 9.5 \text{ M}\Omega$, bulk capacitance $[(C)_b] \sim 557 \text{ nf}$, relaxation frequency $[(f)_r] \sim 300.4 \text{ Hz}$, relaxation time (τ) $\sim 3.3 \text{ ms}$ and DC conductivity $[(\sigma)_{dc}] \sim 6.2 \times 10^{-7} \Omega^{-1} \text{ m}^{-1}$. It can be also satisfied the condition for $2\pi f_0 R_b C_b = 1$. The existence of a step like transitions in the M' imply that the presence of a relaxation process. In this relaxation process is due to the presence of immobile species at lower temperatures and defects/vacancies at higher temperatures.

In this single relaxation coincides with the result of Nyquist plot. The appearance of a peak in the plot of M'' indicates that the transitions occurred from long-range to short-range mobility to increase in frequency²⁵. Also, the peak can provide a clear indication of conductivity relaxation. The maximum frequency ω_{\max} gives the relaxation time τ from the relation $\omega_{\max} \tau = 1$ ²⁴. Generally, distributions of relaxation times were attributed to the difference in the environment surrounding and different ions in a ceramic material. The modulus formalism is an important formalism for characterized the relaxation mechanism in ceramic materials. Figure 8 (a) shows the variation of the real (M') and the imaginary part of the electric modulus (M'') within the frequency region of 1 Hz-100 KHz for the CCTO ceramic. It can be exhibited that the value of M' is very low in the lower frequency region and a sigmoidal increment and reach nearly constant value of M'' in the higher frequency region.

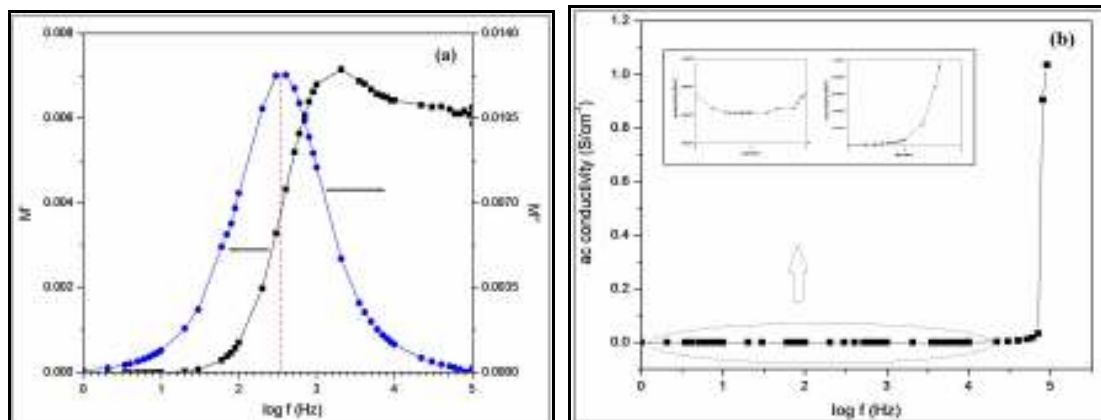


Figure 8.(a)Frequency dependent complex modulus and (b) ac conductivity of CCTO ceramic

The variation of AC electrical conductivity with the frequency of CCTO ceramic sintered at $950 \cdot \text{C}$ for 3 hours is shown in figure 8 (b). It is shown clear that the AC electrical conductivity is frequency independent at lower frequency and dependent nature on higher frequency region. The frequency independent value of AC conductivity (σ_{ac}) corresponds to the DC conductivity (σ_{dc})²⁶. AC electrical conductivity was increased with increased frequency and it confirmed the presence of interfacial effect on CCTO ceramics causes for higher dielectric constant.

Conclusion:

In summary, the cubic system with body-centered lattice of the $\text{CaCu}_3\text{Ti}_4\text{O}_{12}$ nanopowder was successfully synthesized by sol-gel method and confirmed from XRD studies. The amplitude parameters and functional parameters were analyzed from topography image. The FTIR spectrum showed that a mixed vibration of CuO_4 and TiO_6 groups prevailing in the CCTO structure. Optical property of as-synthesized nanopowder was investigated from DRS. The real and imaginary components of the complex impedance and related parameters provided the information about the composition of CCTO ceramic.

Acknowledgements

The Directorate of Extramural Research & Intellectual Property Rights (ER & IPR), Defence Research & Development Organization (DRDO), New Delhi is acknowledged for the financial support (Project No.ERIP/ER/1104613/M/01/1460). The authors are also thankful to Thiru. A. Tenzing, Correspondent and Dr.S.Arivazhagan, Principal, Mepco Schlenk Engineering College, Sivakasi for their constant support and encouragement.

References:

1. Subramanian MA, Li D, Duan N, Reisner BA, Sleight AW. High Dielectric Constant in $\text{ACu}_3\text{Ti}_4\text{O}_{12}$ and $\text{ACu}_3\text{Ti}_3\text{FeO}_{12}$ Phases. *J. Solid State Chem.*, 2000, 151; 323-325.
2. Deschanvres A, Raveau B, Tollemer F. Substitution of Copper for A Divalent Metal in Perovskite-Type Titanates. *Bull.Chim. Soc. Fr.*, 1967: 4077-4078.
3. Bochu B, Deschizeaux MN, Joubert JC. Synthèse Et Caractérisation D'une Série De Titanates Pérowskites Isotypes De $[\text{CaCu}_3](\text{Mn}_4)\text{O}_{12}$. *J. Solid State Chem.* 1979, 29; 291-298.
4. Glazer AM. The Classification of Tilted Octahedra in Perovskites. *Acta Crystall.B.*, 1972, 28; 3384-3392.
5. Homes CC, Vogt T, Shapiro SM, Wakimoto S, Ramirez AP. Optical Response of High-Dielectric-Constant Perovskite-Related Oxide. *Sci.* 2001, 293; 673-676.
6. Ramirez AP, Subramanian MA, Garbel M, Blumberg G, Li D, Vogt T, Shapiro SM. Giant Dielectric Constant Response in a Copper-Titanate. *Solid State Commun.*, 2000, 115; 217-220.
7. Rai AK, Singh NK, Acharya SK, Singh L, Mandal KD. Effect of Tantalum Substitutions On Microstructures and Dielectric Properties of Calcium Copper Titanate ($\text{CaCu}_3\text{Ti}_4\text{O}_{12}$) Ceramic. *Mater. Sci. and Eng. B.*, 2012, 177; 1213-1218.

8. Baral A, Meher KRSP, Varma KBR. Dielectric Relaxation Behaviour of $\text{Sr}_2\text{SbMnO}_6$ Ceramics Fabricated from Nanocrystalline Powders Prepared by Molten Salt Synthesis. *Bull. Mater. Sci.*, 2011, 34; 53–60.
9. Barber P, Balasubramanian S, Anguchamy Y, Gong S, Wibowo A, Gao H, Ploehn HJ, Loye HC. Polymer Composite and Nanocomposite Dielectric Materials for Pulse Power Energy Storage. *Mater.*, 2009, 2; 1697-1733.
10. Jesurani S, Kanagesan S, Velmurugan R, Kalaivani T. A Comparative Study of Conventional Sintering With Microwave Sintering of High Dielectric Calcium Copper Titanate Nano Powder Synthesized by Sol-Gel Route. *Trans. Ind. Ceram. Soc.*, 2011, 70; 79-85.
11. Jesurani S, Kanagesan S, Velmurugan R, Kalaivani T. Phase Formation and High Dielectric Constant of Calcium Copper Titanate using Sol–Gel Route. *J Mater Sci: Mater Electron.*, 2012, 23; 668–674.
12. Hutagalung SD, Mohamed JJ, Ahmad ZA. Lowering Calcination Temperature of $\text{CaCu}_3\text{Ti}_4\text{O}_{12}$ Formation by Modified Mechanic Al Alloying Process. *Emi. J. For Eng. Res.*, 2007, 12; 61-64.
13. Almeida AFL, Oliveira RS, Goes JC, Sasaki JM, Filho AGS, Filho JM, Sombra ASB. Structural Properties of $\text{CaCu}_3\text{Ti}_4\text{O}_{12}$ Obtained by Mechanical Alloying. *Mater.Sci.And Eng. B.*, 2002, 96; 275-283.
14. Fritsch SG, Lebey T, Boulos M, Durand B. Dielectric Properties of $\text{CaCu}_3\text{Ti}_4\text{O}_{12}$ Based Multiphased Ceramics. *J. Eur.Ceram. Soc.*, 2006, 26; 1245-1257.
15. Mote VD, Purushotham Y, Dole V. Williamson-Hall Analysis In Estimation of Lattice Strain in Nanometer-Sized ZnO Particles. *J. Of Theor. And Appl.Phy.*, 2012 6; 6.
16. Jesurani S, Kanagesan S, Velmurugan R, Thirupathi C, Sivakumar M, Kalaivani T. Nanoparticles of the Giant Dielectric Material, Calcium Copper Titanate from a Sol–Gel Technique. *Mater.Lett.*, 2011, 65; 3305–3308.
17. Raposo M, Ferreira Q, Ribeiro PA. A Guide for Atomic Force Microscopy Analysis of Soft-Condensed Mater. *Modern Research and Educational Topics in Microscopy; Formatex.* 2007, 758-769.
18. Willardson R, Beer A. *Optical Properties of III-V Compounds.* Academic Press New York 1967; 318-400.
19. Dressel M, Gruner G. *Electrodynamics of Solids Optical Properties of Electron in Matter.* Cambridge University Press 2002; Pp. 159-65.
20. Ning T, Chen C, Zhou Y, Lu H, Zhang D, Ming H, Yang G. Large Optical Nonlinearity In $\text{CaCu}_3\text{Ti}_4\text{O}_{12}$ Thin Films. *Appl. Phys. A.*, 2009, 94; 567-570.
21. Oliveira RC, Cavalcante LS, Sczancoski JC, Aguiar EC, Espinosa JWM, Varela JA, Pizani PS, Longo E. Synthesis and Photoluminescence Behavior of $\text{Bi}_4\text{Ti}_3\text{O}_{12}$ Powders Obtained by the Complex Polymerization Method. *J. of Alloy. and Comp.*, 2009, 478; 661–670.
22. Ahmed SM, Latif LA, Salim AKH. The Effect of Substrate Temperature on the Optical and Structural Properties of Tin Sulfide Thin Films. *J Basrah Res.*, 2011, 37; 15-20.
23. Bakr NA, Funde AM, Waman VS, Kamble MM, Hawaldar RR, Amalnerkar DP, Gosavi SW, Jadkar SR. Determination of The Optical Parameters of A-Si:H Thin Films Deposited by Hot Wire–Chemical Vapour Deposition Technique using Transmission Spectrum Only. *J. of Phy.*, 2011, 76; 519-531.
24. Barick, Pradhan DK, Choudhary RNP. Ac Impedance Spectroscopy and Conductivity Studies of $\text{Ba}_{0.8}\text{Sr}_{0.2}\text{TiO}_3$ Ceramics. *Advan.Mater. Lett.*, 2011, 2; 419-424.
25. Amarnath K, Prasad K, Chandra KP, Kulkarni AR. Impedance and A.C. Conductivity Studies of $\text{Ba}(\text{Pr}_{1/2}\text{Nb}_{1/2})\text{O}_3$ Ceramic. *Bull. Mater. Sci.*, 2013, 36; 591–599.
26. Sambasiva Rao K, Madhava Prasad D, Murali Krishna P, Swarnalatha T. Structure, Dielectric and Impedance Properties of Barium Strontium Samarium Bismuth Niobate Ceramic. *Ceramics – Silikaty*, 2008, 52; 190-200.
